License

Title: Forces acting on bridge abutments over liquefied ground

All authors and their affiliations:
Akihiro Takahashi, Tokyo Institute of Technology, Tokyo, Japan
Hideki Sugita, Public Works Research Institute, Tsukuba, Japan
Shunsuke Tanimoto, Public Works Research Institute, Tsukuba, Japan

Abstract:
Large earthquake-induced displacements of a bridge abutment can occur, when the bridge is built on a floodplain or reclaimed area, i.e., liquefiable ground, and crosses a water channel. Seismic responses of a bridge abutment on liquefiable ground are the consequence of complex interactions between the abutment and surrounding soils. Therefore identification of the factors dominating the abutment response is important for the development of simplified seismic design methods. This paper presents the results of dynamic three-dimensional finite element analyses of bridge abutments adjacent to a river dike, including the effect of liquefaction of the underlying ground using earthquake motions widely used in Japan. The analysis shows that conventional design methods may underestimate the permanent abutment displacements unless the following two items are considered: (1) softening of the soil beneath the liquefiable layer, due to cyclic shearing of the soil surrounding the piles, and (2) the forces acting on the side faces of the abutment.

Keywords:
abutment, pile foundation, liquefaction, earth pressure, finite element analysis

Soil Dynamics and Earthquake Engineering 30 (3), 146-156, 2010
Original URL:
http://dx.doi.org/10.1016/j.soildyn.2009.10.007

1. Introduction

Large earthquake-induced displacements of a bridge abutment can occur, when the bridge is built on a floodplain or reclaimed area, i.e., liquefiable ground, and crosses a water channel. When the abutment is located adjacent to a river dike or revetment (See Fig. 1), it is especially prone to movement toward the waterfront during an earthquake, when the underlying ground liquefies.

In conventional Japanese design methods, the seismic performance of bridge abutments on liquefiable soil is assessed by pushover analysis, i.e., by calculating the response of the abutment subjected to (1) the inertial force of the superstructure and the abutment, and (2) the seismic active earth pressure of the backfill. The kinematic load induced by interaction between the surrounding soil and structure has been neglected, for simplicity, because liquefaction of the foundation soil appears to cause a reduction of lateral soil resistance [1].

For structures subjected to lateral spread on level ground or gentle slopes, many procedures that account for effects of the lateral spreading on their performance have been proposed [2][3][4][5]. However the existing procedures may not be directly applicable to bridge abutments since the seismic performance of abutments is also affected by many factors, such as, (1) local deformation of the adjacent river dike, (2) deformation of foundation soils caused by the weight of a road embankment connected to the abutment, and (3) slumping of the road embankment itself. Because the seismic response of a bridge abutment on liquefiable ground is the consequence of complex interactions among all these factors, identifying the factors dominating the abutment response is critical when simplified seismic design is used.

In addition, the critical moment for the abutment during earthquakes has to be carefully chosen for such a simplified seismic design method: When the seismic performance of a pile-supported bridge abutment is assessed with the pushover analysis, the response coinciding with the arrival of the largest (principal) shock is generally assumed to represent the critical design condition for the abutment. However, the horizontal displacement of the abutment coinciding with the principal shock is not necessarily the maximum displacement the abutment will experience and the same is also true for the strength and ductility demands for the structural members that form the bridge abutment.

This paper presents the results of dynamic three-dimensional finite element analyses on bridge abutments built on liquefiable ground adjacent to river dikes, taking into account the effect of liquefaction on abutment response. Two configurations of the surrounding ground were modelled, and the seismic response of abutments both with and without piles is presented. Forces acting on the abutment as well as calculated responses of the abutment are described in detail to demonstrate

(1) the critical moment assumed in the conventional design methods, i.e., pushover analyses, being not always appropriate and (2) marked contribution of the forces acting on the side faces of the abutment in the forces acting on the abutment. The results of the analyses are presented, including recommendations for revisions in the current conventional design methods employing the pushover analysis for bridge abutments.

2. Numerical analysis overview

Highway bridge abutments constructed near a river channel were modelled and analyzed. Two configurations of the ground surrounding the abutment were considered; a plan view and cross section of the models is illustrated in Fig. 2. The bridge crosses a river, with a distance between abutments of 70m. For a fully coupled three-dimensional finite element analysis, limited computer resources did not permit the use of a fine mesh, so a relatively coarse mesh was employed (cf. Fig. 6 in the following section). Because of this limitation, the pile foundation was modelled by relatively small number of piles having large diameter.; The pile foundation was modelled with six D=2m x L=20m cast-in-place concrete piles, arranged in 2x3 grids with 5m spacing. The width of the bridge is 15m, and the slope of the river dike and road embankment connected to the 10m-high pile-supported abutment is 1V:2H. The water level was set at 7.5m below the crest of the dike. The original ground level is 5m above riverbed for the cases illustrated in Fig. 2(a), and 10m for the cases shown in Fig. 2(b). The thickness of the liquefiable layer (loose sand deposit) below the water table is 12.5m, and the materials of the dike and embankment are assumed to be the same as that of the surface layer that lies above the water table. The piles are installed into a bottom non-liquefiable layer (dense sand deposit) through the liquefiable layer.

In the numerical analyses, only a half-width of the road bridge in the y-direction was modelled, in order to take advantage of symmetry. The width of the analytical domain in y-direction is 100m, the length in x-direction is 240m, and the depth in z-direction from the riverbed is 20m. The x=−40m and x=200m planes were allowed to move freely in the x- and z-directions, but not in the y-direction. At z=−20m, all movement was restrained. Fluid flow velocities normal to the analytical domain boundary were set to zero at the side and bottom boundaries. Soils, stem and base of the abutment were modelled by solid elements, and the piles were modelled with elastic beam elements. Because Potyondy [6] reported that the wall friction angle between smooth concrete and sand is around 75% of the soil shearing resistance, no interface element was inserted between the abutment and the adjacent soil. The extended sub-loading surface model proposed by Hashiguchi & Chen [7] was adopted for the soil layers. Material parameters of the soil layers and the structural components are listed in Table 1, where Gs=specific gravity, e_0=initial void ratio, λ & κ=slopes of the compression & swelling lines in v-ln(p') plane, ν=Poisson's ratio, k=hydraulic conductivity, ρ=unit density, E=Young's modulus, I=flexural rigidity of the beam, A=area of beam section, and the other parameters are specific parameters for the constitutive model used. Liquefaction resistances of the non-liquefiable and liquefiable layers are summarized as the cyclic shear stress ratio plotted against the number of loading cycles that cause liquefaction in triaxial tests, as shown in Fig. 3. Typical stress path and stress-strain relations for the liquefiable layer soil are shown in Fig. 4. Details of the numerical analysis code are described in Takahashi [8].

To evaluate the seismic performance of structures, two levels of earthquake motions are used in Japan [9]; one is a moderate earthquake motion whose return period is smaller than the life time of a structure (from 50 to 100 years) and the others are strong earthquake motions whose return period is more than several hundred years. For the latter, two types of earthquake motions are considered; one is the inland earthquake motion and the other is the subduction earthquake motion. In this study, numerical analyses were performed to assess the seismic performance of the bridge abutments against the strong earthquakes. Figure 5 shows the applied earthquake motions. These are widely used in practice in Japan. One is the inland earthquake motion (Fig. 5(a), sample waveform for Spectrum II [10].) The other one is the subduction earthquake motion (Fig. 5(b), sample waveform for Spectrum I [10].) The earthquake motion is applied in the bridge axis direction (x-direction). The equations of motion are integrated using Newmark's β method, with a time step Δt=0.005 sec. System damping is represented by Rayleigh damping using a damping ratio of 2.5 % in a first mode of free vibration of the system.

Six calculations were conducted, as listed in Table 2. Except for P-H(EQ1), the inland earthquake motion (Fig. 5(a)) was applied. Before performing a dynamic response analysis, a geostatic analysis was conducted, by applying the self weight gradually, in order to establish the initial stress state of the system. In P-L, the road embankment was connected to the pile-supported abutment, with the original ground level set to a height of 5m above the riverbed (Fig. 2(a).) For this case, waterward and landward stretching of the river dike, and the slumping of the road embankment, were expected. In P-H, because the ground level was set to a height of 10m above the riverbed (at the same level of the roadway, Fig. 2(b),), the deformation mode of the surrounding ground was thought to be simpler than for case P-L, since no complicated spreading mode of the foundation ground, induced by the slumping of the road embankment in a direction perpendicular to the bridge axis, was expected. By comparing cases P-L and P-H, the effect that the geometry of the surrounding ground has on the seismic response of the abutment can be observed.

In case P-H(Fix), the "strut effect" of the bridge deck on abutment response was modelled by constraining the horizontal displacement of the top of the abutment. In the geostatic analysis, it was assumed that the top of the abutment is initially in contact with the deck before shaking commences for all the cases. Thus, the initial stress state of the system for P-H(Fix) is the same as that for the case without the strut effect (P-H). Since the critical moment in the abutment may vary depending upon the earthquake motion waveform, the subduction earthquake motion (Fig. 5(b)) is applied in P-H(EQ1). For comparison, responses of the abutment without piles are calculated in NP-L and NP-H.

The limitations of the analysis are: (1) the bridge deck and intermediate piers were not modelled, and (2) the top of the abutment was free to move, without restriction, except in case P-H(Fix). In other words, the dynamic interaction between the deck and the abutment was not modelled, because our main concern was the interaction between the abutment, foundation ground, road embankment, and river dike. As a result of these limitations, the calculated displacements and vibration modes of the abutment may be different from those in a real bridge-foundation system. In addition, since the only the two waveforms are considered, the observation on numerical analyses in this study has to be taken as one of the examples. Even though we label one of the input motions as the inland earthquake motion and the other as the subduction earthquake motion, the used motions are not necessarily representative waveforms for these types of motions.

3. Observations on numerical analyses

In conventional Japanese design methods, seismic responses of an abutment are typically calculated by the pushover analysis assuming that (1) the response coinciding with the arrival of a principal shock represents the critical design condition for an abutment and (2) effects of the lateral spreading on the abutment response are negligible. In this section, these major assumptions in the conventional design methods are examined through observations on numerical analyses.

3.1. Permanent deformation of the ground surrounding the abutment

Ground deformations around the pile-supported abutment (P-L & P-H) at *t*=30sec (when ground shaking almost ceases) are drawn in Fig. 6. Large shear deformation of the loose sand deposit under the abutment and the connected road embankment (the roadway for P-H) was observed in both cases. In the case where the original ground level was lower than the height of the river dike crest (P-L), the road embankment showed relatively large settlements, with marked uneven settlement occurring just above the heel of the abutment pile cap. In addition, the shear deformation of the liquefiable layer under the road embankment is somewhat smaller than for case

P-H.

The waterward horizontal displacements of the river dike far from the abutment are not affected by abutment movement. The higher the original ground level, the larger the waterward permanent horizontal displacement of the dike, i.e., the lateral spread. On the other hand, the deformation of the rive dike near the abutment are restrained by the abutment. Due to this restriction, the backfill behind the abutment shows permanent horizontal displacement normal to the bridge axis (see the horizontal ground displacement at the river dike's crest level, the lower graphs in Fig. 6). Although the plots for the abutments without piles (NP-L & NP-H) are not shown here, they are approximately the same as those for the pile-supported abutment, except for abutment tilting (large tilting of the abutment was seen in NP-L & NP-H) and relative horizontal displacement between the dike and the abutment (the relative displacement was not large in these cases).

3.2. Excess pore water pressure response

Although the above-mentioned permanent deformations of the abutment and surrounding ground were caused by the generation of the excess pore water pressure in the loose sand deposit, this does not necessarily mean that full liquefaction took place over the entire area. In P-L, the loose sand just below the dike and embankment was not fully liquefied, whereas full liquefaction did occur in other areas, as shown in Fig. 7. There are two possible reasons for this: one reason is that the embankment (including the river dike) load on the foundation ground induced shear stress in the foundation soil, increasing its strength against cyclic shear stress [11]. The other reason is that the smaller overburden pressure at the original ground surface limits the excess pore water pressure that can develop in the liquefiable layer, resulting in water migration from the embankment foundation toward the original ground, thereby reducing the excess pore water pressure in the embankment foundation.

The liquefiable layer under the roadway is also liquefied in P-H, since it does not meet the conditions mentioned above, i.e., unlike P-L, there is no initial shear stress in the plane normal to the bridge axis and no ground water migration from the embankment foundation toward the original ground. For the cases on the non-pile-supported abutment (NP-L & NP-H), the excess pore water pressure ratio just below the abutment is very small, compared to the pile-supported abutment, due to the large confining pressure induced by the abutment weight (for the pile-supported abutment cases, the weight of the abutment is supported by piles, and does not contribute to increasing the confining stress of the liquefiable soil underneath the abutment.)

3.3. Horizontal abutment displacement

Figure 8 shows the time histories of the horizontal displacement of the top of the abutment for all cases except P-H(Fix) (the horizontal displacement of the abutment top is constrained in that case), together with the time histories of the channel-side shoulder of the dike far from the abutment (x=-5m, y=100m & z=10m), shown with a dashed line. Negative values of displacement represent waterward abutment movement. When the inland earthquake is applied, the horizontal displacement of the abutment increases with shaking; two large fluctuations in the horizontal displacement time histories coincide with the two large shocks in the input motion (see Fig. 5). For the subduction earthquake, P-H(EQ1), the displacement time history does not show a large jump during the principal shock, and the displacement increases monotonically with the shaking. The permanent displacements of the pile-supported abutments (P-L & P-H) are smaller than those of the abutments without piles (NP-L & NP-H), and the higher the original ground level (for the cases with the surrounding ground geometry shown in Fig. 2(b)), the larger the abutment horizontal displacement. For all the cases the permanent abutment displacement is larger than the displacement that occurs at the time of the principal shock.

The horizontal displacements of the river dike far from the abutment are not affected by abutment movement (cf. (1) P-L & NP-L and (2) P-H & NP-H) as mentioned before. The higher the original ground level, the larger the permanent horizontal displacement of the dike, i.e., the lateral spread. The larger resistance of the abutment foundation against spreading results in a larger relative displacement between the abutment and the spreading ground. In the pile-supported abutment cases, the relative displacement is large, whereas it is very small for the abutments without piles. Restraint of the ground around the abutment against spreading causes the forces acting on the abutment to be larger, and affects the strength and ductility demands that are made on the structural members.

3.4. Earth pressure acting on abutment back face

Figure 9 shows the time histories of the coefficient of horizontal earth pressure acting on the abutment back face (x=5m). The coefficient is defined as an average ratio of the horizontal effective stress to the vertical effective stress. Before the arrival of the principal shock, the earth pressure acting on the back face of the abutment decreases slightly with increasing abutment displacement. The earth pressure time histories show sharp spikes (the maximum earth pressures that occurred during the entire shaking history) coinciding with the arrival of the first principal shock. After the first principal shock, the earth pressure decreased to a nearly constant level when subjected with the inland earthquake motion; when subjected to the subduction earthquake (P-H(EQ1)), the maximum earth pressure does not coincide with the principal shock.

In Fig. 9, the coefficients calculated by the Mononobe-Okabe method are shown with arrows. For the cases without piles (NP cases) and the pile-supported abutment case with a lower original ground level (P-L), the maximum values are approximately equal to the Mononobe-Okabe values, while in the P-H cases, especially when constrained against horizontal displacement (P-H(Fix)), the maximum values were larger than the Mononobe-Okabe. In the former cases, the earth pressure coefficient following the principal shock is smaller (close to the active earth pressure coefficient), whereas it is relatively large in the latter cases. Even in the case when the top of the abutment is restrained (P-H(Fix)), the values are far below potential passive earth pressures.

These observations are linked to the relative displacements between the abutments and the spreading ground. When either (1) the abutment foundation has a small amount of restraint against movement toward the waterfront (NP cases), or (2) the lateral spread is relatively small because of a lower original ground level (P-L), the relative displacement is small and the spread-induced component of earth pressure is also small. In these cases, the peak earth pressure can be approximated by the Mononobe-Okabe method, and the earth pressure remaining following shaking is small. For the cases with larger relative displacements, since the spread-induced component of earth pressure is relatively large, the peak earth pressures can be larger than the Mononobe-Okabe value.

When the seismic performance of a pile-supported bridge abutment is analyzed with the conventional Japanese design methods, the response coinciding with the arrival of the largest (principal) shock is generally assumed to represent the critical design condition for the abutment. However, our observations have shown that the horizontal displacement of the abutment coinciding with the principal shock is not necessarily the maximum displacement the abutment will experience. These observations underscore the importance of taking into account the permanent deformations of the surrounding ground.

3.5. Bending moment of piles

Bending moment diagrams for the piles, corresponding to the time when the abutments experience maximum earth pressure, are plotted in Fig. 10 (for P-L, P-H, PH(Fix) & P-H(EQ1)). Envelopes of the maximum and minimum bending moment are also shown, with dashed lines, in the figure, along with the bending moment at the end of the shaking. These diagrams show the average moment of the pile group, because there is very little variation between the moments in all the piles in the group. In every case, the large bending moment occurs at the pile head (z=0m) and at the interface between the liquefiable and non-liquefiable layers (z=10m). When the abutment top is constrained against horizontal displacement (P-H(Fix)), the maximum and minimum bending moments are very small compared to the moments in the unconstrained abutments.

For the cases subjected to the inland earthquake motion, the maximum earth pressure acting on the back face of the abutment occurs at t=10.88sec (cf. Fig. 9), and the inertia force of the abutment reaches its maximum value slightly before this time. For the case with the subduction earthquake motion, P-H(EQ1), the maximum earth pressure during the principal shock appears at t=27.52sec, which almost coincides with the maximum inertia force of the abutment, while the maximum throughout the shaking is at t=37.60sec. This is probably due to semi-long-period components of input motion that follows the principal shock (a wave undulation with a period of about 2~3sec can be seen following the principal shock in Fig. 5(b)). The fluctuation in the earth pressure induced by this semi-long-period component of input motion, along with the forces that have already been induced by significant lateral spreading, may have put the piles into a critical stress condition for the case with the subduction earthquake motion.

For all the cases, when the earth pressure acting on the abutment is maximum, the bending moment at z=0m and z=10m is approximately equal to the maximum and minimum bending moments that occur throughout the shaking. For cases in which the maximum earth pressure acting on the abutment back face occurs at about the same time that the maximum inertia force occurs, (i.e., the cases with the inland earthquake motion), the critical bending moment in the piles coincides with the maximum inertia force; however, this is not true for the subduction earthquake case.

These results suggest that for the inland earthquake, critical pile bending moments can be determined by the pushover analysis (even though maximum abutment displacements cannot be determined by conventional methods). But when the critical bending moment in the piles is caused by lateral spreading that occurs after the principal shock (such as in the subduction earthquake with a relatively small peak motion but with a duration long enough to cause lateral spreading), neither the maximum pile bending moments nor the maximum abutment displacements can be assessed with the pushover analysis.

4. Forces acting on the abutment

The numerical analyses reveal that when the earth pressure acting on the back face (not the inertia force) of the abutment is maximum, the piles are experiencing their critical strength/ductility demand, even though the horizontal displacement of the abutment may not have reached its maximum value yet. Although the maximum earth pressure occurs at the same time as the critical bending moment in the piles, this does not necessarily mean that the earth pressure acting on the back face of the abutment is the cause of the critical bending moment in the piles. In this section, other components of the forces acting on the abutment are examined, in order to identify relevant forces dominating bridge abutment response for conventional seismic design methods.

With regard to spreading soils, the abutment acts as a restraint against lateral spread; in other words, the forces acting on the abutment are the result of interaction between the spreading soils and the pile foundation. The NCHRP 472 Recommended Specifications for Seismic Design of Bridges [12][13] implemented this concept by formulating a simplified procedure for calculating the response of an abutment over liquefied ground, and Boulanger et al. [14] applied this procedure to a physical model test. First, we will present the analysis results in a form similar to that used in the NCHRP 472, and then we will analyze the contribution of each component of the force acting on the abutment.

Figure 11 shows plots of the average foundation resisting forces, F_R/B, against the horizontal displacement of the abutment base for P-L, P-H, P-H(EQ1), NP-L & NP-H. For the abutments without piles, the resisting force is calculated by integrating the shear stress on the foundation base caused by frictional resistance. The resisting force of the pile-supported abutments is determined by summing the shear forces at the pile heads (the frictional resistance of the foundation soil is negligible for these cases). The average resisting force corresponds to the foundation resistance per unit width of the abutment. The points at the end of shaking are indicated by triangles, and the times of the maximum earth pressure acting on the abutment back face is shown by double circles.

For the cases subjected to the inland earthquake motion (P-L, P-H, NP-L & NP-H), the foundation resisting forces act to restrain the spreading soils. Therefore, the larger the foundation resisting force, the smaller the permanent abutment displacement, as shown in the figure. The chain lines in the figure represent the abutment displacement curves subjected to various restraining forces, and the triangles correspond to points where the displacement of the pile foundation and the abutment are compatible.

The foundation resistance coinciding with the maximum earth pressure acting on the back face of the abutment (the double circle points) does not seem to depend on the geometry of the surrounding ground, but instead depends on the foundation type. However, the backbone curve depends on both ground geometry and foundation type, for the cases subjected to the inland earthquake motion. The slope of the backbone curves decreases with shaking, that is, it decreases with the relative displacement. The average shear forces are plotted against the horizontal pile displacement at a depth of 8.75m (just above the interface between the liquefiable and non-liquefiable layers) for P-L, P-H & P-H(EQ1), shown in Fig. 12. These figures indicate that the decrease in the slope of the backbone curve that takes place as the shaking progresses may be caused by softening of the soils in both the liquefiable layer and in the bottom non-liquefiable layer, due to the cyclic shearing of the soil surrounding the piles. This cyclic softening effect in a soil layer lying beneath a liquefiable layer is not ordinarily considered in pushover analyses, which might, therefore, underestimate actual abutment displacements.

Comparisons between Figs. 11 and 12 bring to light the following points: (1) large changes in the shear force at the pile head during the first shock are not seen in the vicinity of the interface between the liquefiable and non-liquefiable layers, for the cases with the inland earthquake motion, and (2) after the principal shock, the shear forces near that interface are slightly larger than the shear forces at the pile head. The first observation indicates that the dynamic load delivered by the pile heads during the first shock is resisted primarily by the liquefiable layer, and is not transmitted to the bottom non-liquefiable layer. Figure 13 shows the stress paths of the liquefiable soil element adjacent to the piles (x=1.25m, y=3.75m & z=-6.25m) for P-L & P-H. The large resistance of the liquefiable layer at that point in time may be attributed to the dilative behaviour of the soil, as shown in Fig. 13. The latter observation illustrates the existence of the waterward lateral forces against the piles at the liquefiable layer, due to the lateral spread. Although this is not insignificant, we will not discuss this phenomenon any further, because our main concern here is the forces acting on the abutment.

The foundation resisting force, $F_R = F_I + (F_B - F_F) + 2F_S$ is a reaction to the forces acting on the abutment (see Fig. 14) where F_B is the forces acting on the back face of the abutment, F_F on the front face, F_S on the side faces, and F_S is the inertia force. All forces except F_I are affected not only by dynamic soil-structure interaction, but also by the spreading soils. Examining the contributions of these forces to the abutment response is of value for purposes of improving the current design method, because identification and consideration of the relevant factors dominating bridge abutment response is important in the simplified design methods. This is of value not only for performance assessment of the foundation itself, but also for assessing the soils surrounding the abutment, since these forces are also acting to restrain the spreading soils.

Changes of the forces mentioned above for P-H are shown in Fig. 15. The inertia force dominates the group of forces acting on the abutment during the principal shock. The forces acting on the back face and side faces of the abutment increase with shaking, but the forces on the front face decrease. Similar plots for NP-H are shown in Fig. 16. In this case, the forces acting on the side faces are negligible. Changes in the sum of these forces, and (1) changes in the shear forces acting at the pile head for P-H, or (2) changes in the integrated shear stress of the foundation soil for NP-H, are plotted in the bottom of the figures. Since, (1) the force acting on a face of the abutment is calculated by integrating the stresses in the soil elements that contact the abutment face of interest, and since (2) the shear force in the beam element connected to the abutment base is affected by the nodal forces acting on the opposite side of the pile heads, these forces were not exactly identical, although they were of the same order of magnitude (with an error of about 20%). Therefore, the contribution of each force acting on the abutment was determined by proportion, so that the contributing forces add up to the total force.

Table 3 summarizes contribution ratios of the forces acting on the abutment at the time the maximum earth pressure acting on the abutment back face occurs, for P-L, P-H, P-H(EQ1), NP-L & NP-H. For the cases with the inland earthquake, the inertia force is the dominant force acting on the abutment base. The contribution of the force acting on the abutment side face is very small for the pile-supported abutments (P-L & P-H), while it is relatively large for the abutments without piles (NP-L & NP-H). For the case of the subduction earthquake, P-H(EQ1), the ground has already been subjected to number of shearing cycles before arrival of the large earth pressure acting on the back face. This results in a smaller inertia force, and the other components contribute more to the total force acting on the abutment base.

A similar summary for the end of shaking is shown in Table 4. For the pile-supported abutment, the contributions of the forces acting on the abutment back face and front face $\left(F_B - F_F\right)$ are the greatest, but there are also significant contributions of force from the side faces, especially when the original ground level is high (P-H & P-H(EQ1)). However, the force acting on the side faces is negative (the adjacent river dike behaving as a resistance) for the cases without piles and its absolute value is larger for the case with the lower original ground level (NP-L). This is related to the relative displacement between the abutment and the spreading ground at the end of shaking, i.e., the larger the relative displacement, the larger the contribution of the force acting on the side faces (cf. Fig. 8). Figure 17 is a plot of the forces acting on the side faces against the relative displacement between the abutment and the spreading ground, for all the cases. The coefficient of the force acting on the side faces is defined as a ratio of F_S to $\int_0^H L(z)\rho' g dz$, where z=depth from the abutment top, $L(z)$=length of abutment in the bridge axis direction at a depth of z (i.e., the average ratio of the shear stress to the initial vertical stress). The force is uniquely related to the relative displacement, and its upper limit seems to be a coefficient of about 0.5 in this study.

These observations suggest that, (1) the inertia force dominates the force acting on the abutment base when the peak of an earthquake motion arrives before occurrence of the major spreading of the surrounding ground, (2) the greater the restraining force of the abutment foundation, i.e., the larger the relative displacement between the abutment and spreading ground, the larger the contribution of the force acting on the abutment side faces until the side drag force reaches its ultimate value. Conventional design methods employing the pushover analysis for the abutment response calculation could underestimate permanent abutment displacements, unless (1) the softening of the soil in the layers beneath the liquefiable layer, caused by the cyclic shearing of the soils surrounding piles, and (2) the force acting on the abutment side faces, are taken into account. Due consideration of these factors is recommended in order to realistically assess permanent abutment displacements.

5. Conclusions

This paper presents the results of dynamic three-dimensional finite element analyses of bridge abutments adjacent to a river dike, including the effect of liquefaction of the underlying ground using earthquake motions widely used in Japan. We examined the validity of assumptions in the conventional design methods with the pushover analysis and identified the factors dominating the abutment response through the numerical analyses. Based on the analysis results and discussion, the following conclusions can be drawn:

(1) The permanent displacements of pile-supported abutments in liquefied ground are smaller than the displacements of abutments without piles, as expected. Irrespective of the foundation type and elevation of the ground behind the river dike, the abutment displacement that occurs with the principal shock of an earthquake is not the maximum displacement; the final abutment displacement following the earthquake will be larger.

(2) The piles supporting the abutment are structurally critical at the time of the maximum earth pressure acting on the back face of the abutment for both the inland earthquake and the subduction earthquake, even though the dynamics of these two types of earthquakes are completely different. For the inland earthquake, the maximum earth pressure coincides with the peak of the principal shock of the earthquake. At that time, the piles are in a critical condition, because the inertia force that dominates the forces acting on the abutment (about 70%) is close to the maximum. For the subduction earthquake, the major lateral spreading has already started before the peak earthquake motion arrives, and the forces induced by soil spreading (about 80%) overshadow the maximum inertia force (about 20%). A semi-long-period component of input motion following the principal shock causes large fluctuations in the earth pressure. This fluctuation, along with the forces that have already been induced by significant lateral spreading, puts the piles into a critical stress condition when this type of earthquake is considered.

(3) The foundation resisting force is a reaction to the combined forces acting on the abutment,

including the forces acting on the abutment back face, on the front face, on the side faces, and the inertia force. Except for the inertia force, these forces are affected by the soil spreading. The forces acting on the back face and side faces of the abutment increase as the relative displacement between the abutment and spreading ground far from the abutment increases. The contribution of the force acting on the side faces increases along with this relative displacement. In this study, the force acting on the sides faces at the end of shaking is around 30-40% for pile-supported abutments, whereas this same force is negligible or negative (acting as resistance for the abutment) without piles.

(4) Conventional design methods employing the pushover analysis could underestimate the permanent abutment displacement unless (1) the softening of the soil in the layers beneath the liquefiable layer, due to the cyclic shearing of the soil surrounding the piles, and (2) the force acting on the abutment side faces, are taken into account. Inclusion of these factors is recommended for assessing permanent abutment displacements.

References

1. Shirato, M., Fukui, J. & Koseki, J. 2006. Current status of ductility design of abutment foundations against large earthquake, Soils and Foundations, Vol.46, No.3, 377-396.
2. Japan Road Association. 2002. Specifications for highway bridges, Part V, Seismic design, Maruzen, Tokyo.
3. Dobry, R., Abdoun, T., O'Rourke, T.D. & Goh, S.H. 2003. Single piles in lateral spreads: Filed bending moment evaluation, Journal of Geotechnical and Geoemvironmental Engineering, ASCE, Vol.129, No.10, 879-889.
4. Cubrinovski, M. & Ishihara, K. 2004. Simplified method for analysis of piles undergoing lateral spreading in liquefied soils, Soils and Foundations, Vol.44, No.5, 119-133.
5. Takahashi, A., Sugita, H. & Tanimoto, S. 2006. Beam on Winkler foundation method for piles in laterally spreading soils, ASCE Geotechnical Special Publication, No. 145, 230-241.
6. Potyondy, J.G. 1961. Skin friction between various soils and construction materials. Geotechnique, Vol.11, No.4, 339-363.
7. Hashiguchi, K. & Chen, Z.P. 1998. Elastoplastic constitutive equation of soils with the subloading surface and the rotational hardening. International Journal for Numerical and Analytical Methods in Geomechanics, Vol.22, 197-277.
8. Takahashi, A. 2002. Soilñpile interaction in liquefaction-induced lateral spreading of soils, DEng. Dissertation, Tokyo Institute of Technology.
9. Japan Society of Civil Engineers. 2000. Earthquake resistant design codes in Japan, Maruzen,

Tokyo.
10. Railway Technical Research Institute. 1999. Seismic design for railway structures, Maruzen, Tokyo (in Japanese).
11. Rollins, K.M. & Seed, H.B. 1990. Influence of buildings on potential liquefaction damage, J. Geotechnical Engineering, ASCE, Vol.116, No.2, 165-185.
12. Martin, G.R., March, M.L., Anderson, D.G., Mayes, R.L. & Power, M.S. 2002. Recommended design approach for liquefaction induced lateral spreads, Proc. 3rd National seismic Conference and workshop on bridges and highways, MCEER-02-SP04, Buffalo, NY.
13. Transportation Research Board, National Research Council. 2002. Comprehensive specification for the seismic design of bridges, National Cooperative Highway Research Program, Report No.472, National Academy Press.
14. Boulanger, R.W., Chang, D., Gulerce, U., Brandenberg, S.J. 2006. Evaluating pile pining effects on abutments over liquefied ground, ASCE Geotechnical Special Publication, No. 145, 306-318.

Table 1: Material parameters

(a) For soil layers

Parameter	Non-liquefiable layer (Dense sand deposit)	Liquefiable layer (Loose sand deposit)	Surface layer
G_s	2.65	2.68	2.68
e_0	0.65	0.85	0.85
κ	0.00054	0.00090	0.00090
λ	0.0072	0.019	0.019
ν	0.333	0.333	0.333
ϕ	41.3°	38°	38°
ϕ_d	27°	27°	27°
μ	0.5	1.0	0.0
ϕ_b	19.5°	19.5°	19.5°
b_r	2000	400	400
u_1	2	2	2
m_1	1	1	1
c	10	30	30
K_0	0.5	0.5	0.5
s_{ij0}	$0.7\sigma_{ij0}$	$0.2\sigma_{ij0}$	$0.2\sigma_{ij0}$
OCR	16	2	2
k (m/s)	5×10^{-4}	5×10^{-4}	–

(b) For abutment

Parameter	ρ (Mg/m^3)	EI (GN.m^2)	EA (GN)	E (GPa)	ν
Pile	2.5	4.2	79	–	–
Abutment	2.5	–	–	21	0.3

Table 2: Analysis conditions

Case	Abutment	Ground level from riverbed*	
P-L	w/ piles	5m	
P-H	w/ piles	10m	
P-H(Fix)	w/ piles	10m	Horizontal displacement of abutment top is constrained.
P-H(EQ1)	w/ piles	10m	Spectrum I earthquake motion (Fig. 5(b)) is applied.
NP-L	w/o piles	5m	
NP-H	w/o piles	10m	

* Geometry of surrounding ground for 5m is illustrated in Fig. 2(a) and that for 10m is in Fig.2(b).

Table 3: Contribution ratios of the forces acting on the abutment at time of maximum earth pressure acting on abutment back face

Case	P-L	P-H	NP-L	NP-H	P-H(EQ1)	
Time: sec	10.88				27.52*1	37.60*2
$(F_B - F_F)/F_R$	25%	24%	19%	25%	54%	57%
$2F_S/F_R$	3%	6%	8%	12%	25%	36%
F_I/F_R	73%	70%	73%	64%	21%	7%

*1: At time of maximal earth pressure during principal shock

*2: At time of maximum earth pressure throughout shaking

Table 4: Contribution ratios of the forces acting on the abutment at end of shaking

Case	P-L	P-H	NP-L	NP-H	P-H(EQ1)
$(F_B - F_F)/F_R$	72%	59%	142%	105%	61%
$2F_S/F_R$	28%	41%	-42%	-5%	39%

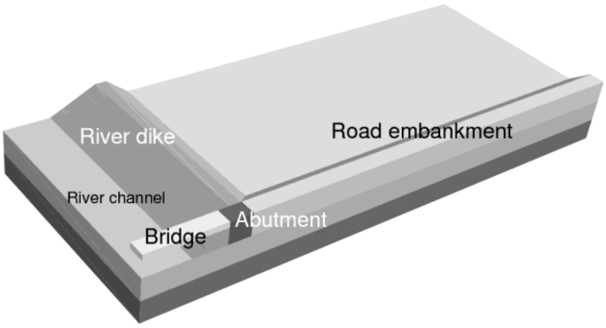

Fig. 1: Bird's eye view of abutment for river crossing bridge

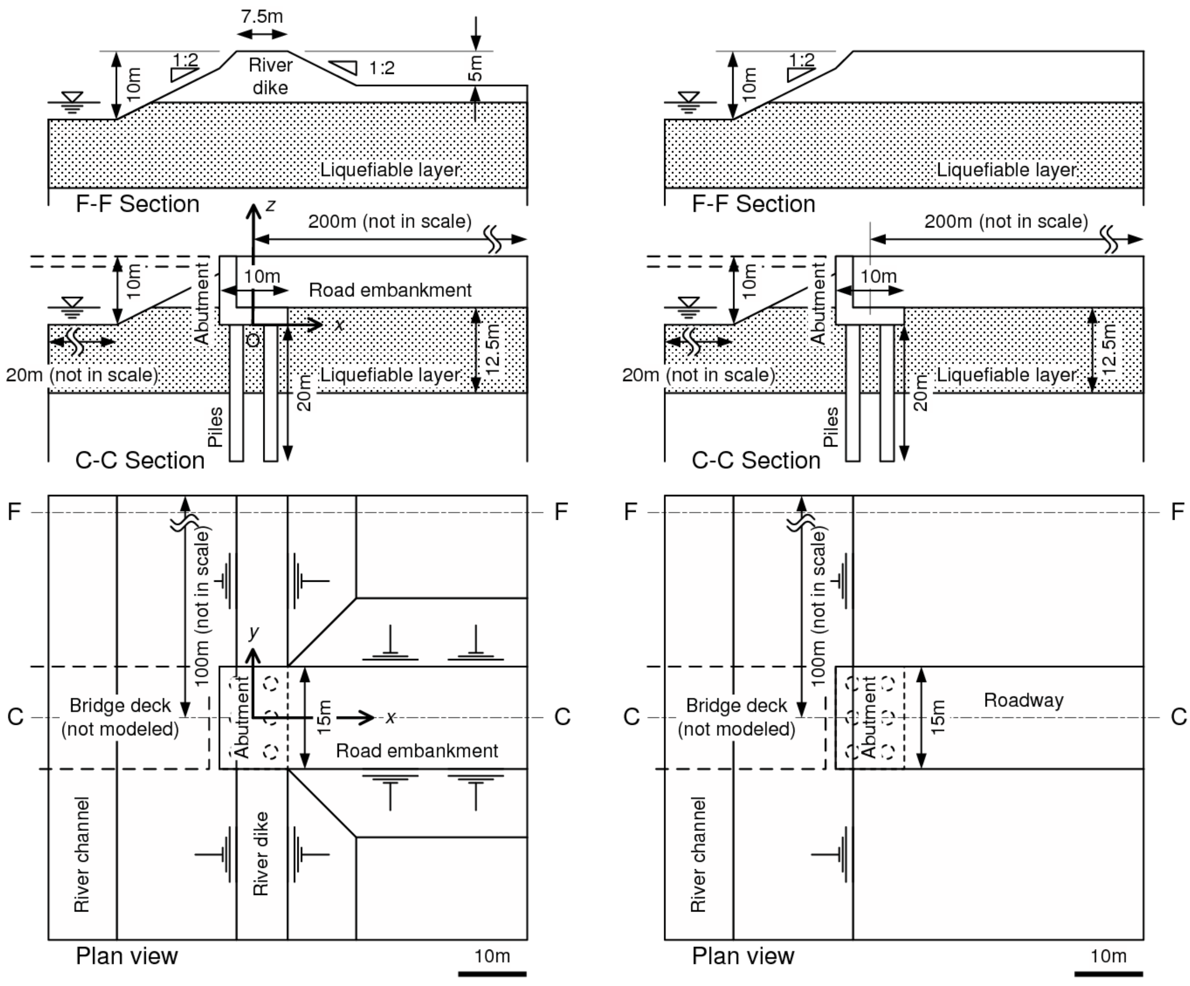

(a) Ground level is at a height of 5m above riverbed (P-L & NP-L)

(b) Ground level is at a height of 10m above riverbed (P-H & NP-H)

Fig. 2: Plan views and cross sections of target abutments

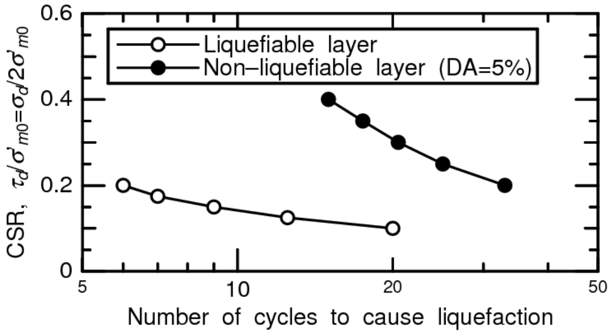

Fig. 3: Relationship between cyclic stress ratio and number of cycles to cause liquefaction

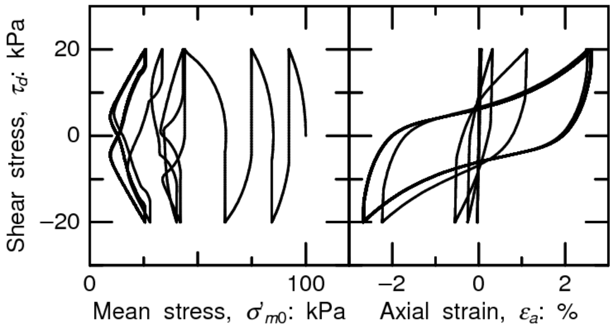

Fig. 4: Typical stress path and stress-strain curves for liquefiable layer soil

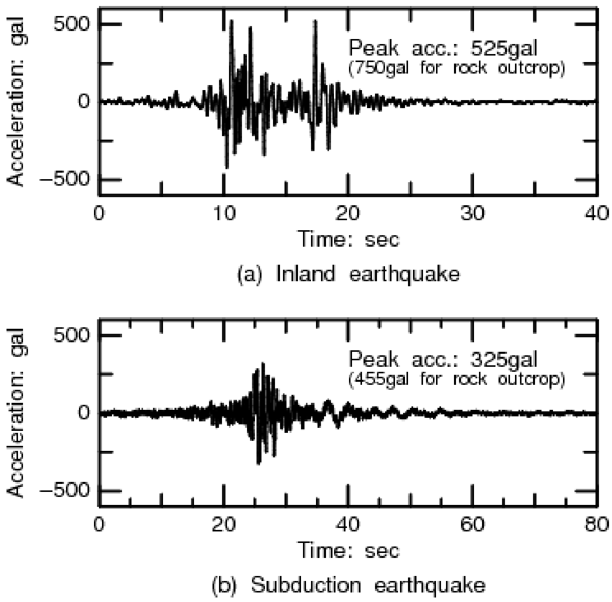

Fig. 5: Applied earthquake motion time histories

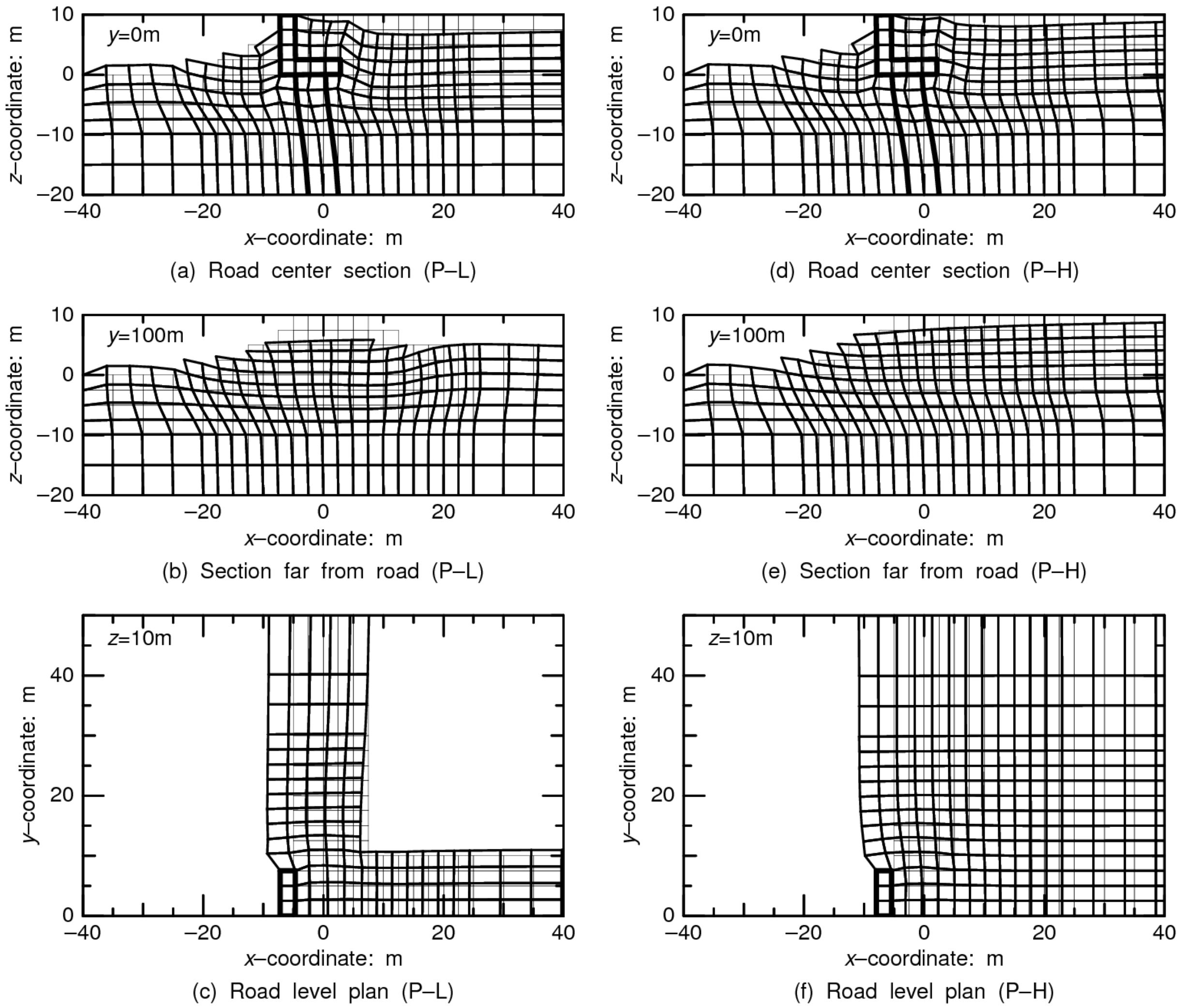

Fig. 6: Ground deformations around piled abutment, where displacement scale is magnified by a factor of ten for P-L (Left) and P-H (right) at t=30sec

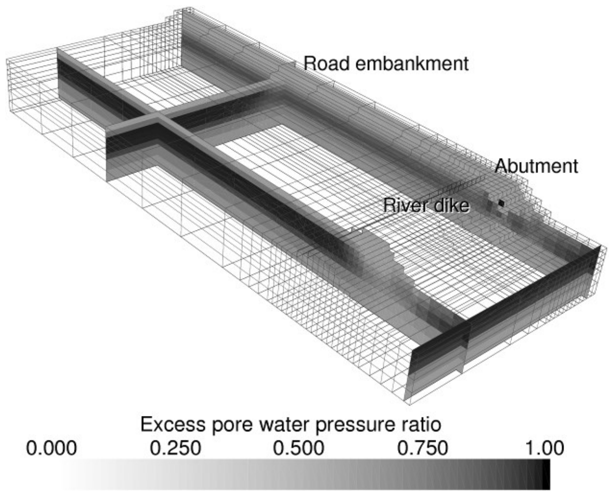

Fig. 7: Excess pore water pressure ratio contours at t=20sec for P-L

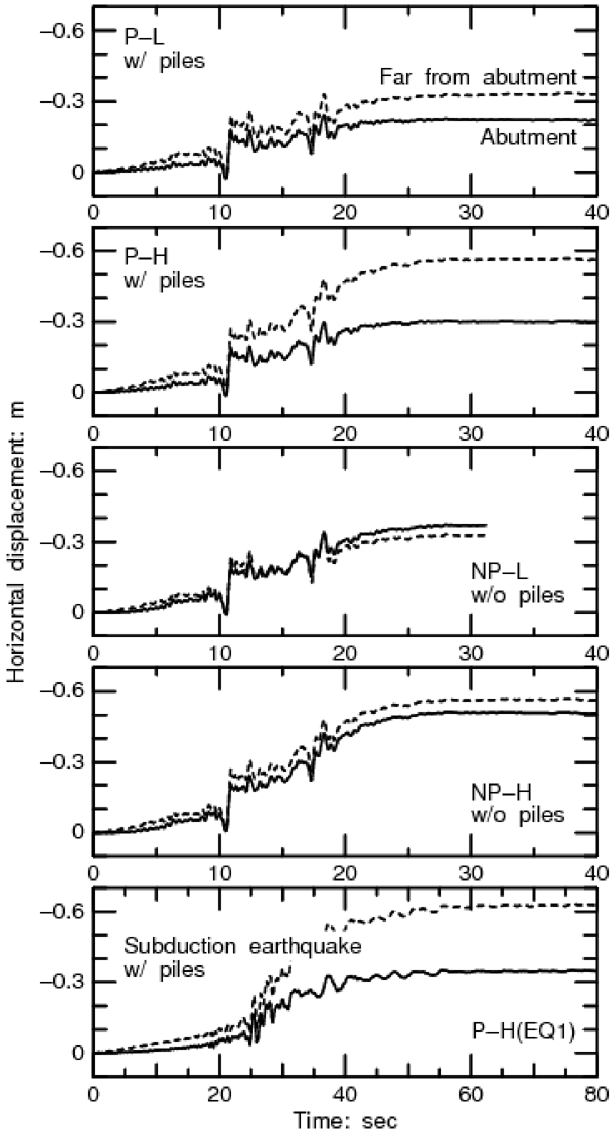

Fig. 8: Time histories of horizontal displacement of abutment top

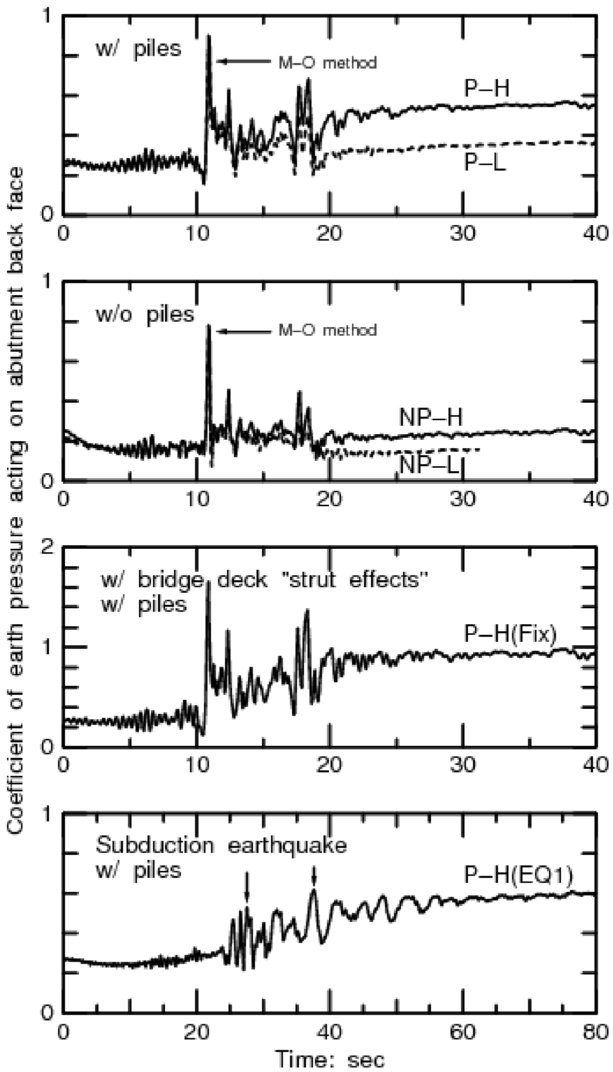

Fig. 9: Time histories of coefficient of earth pressure acting on abutment back face

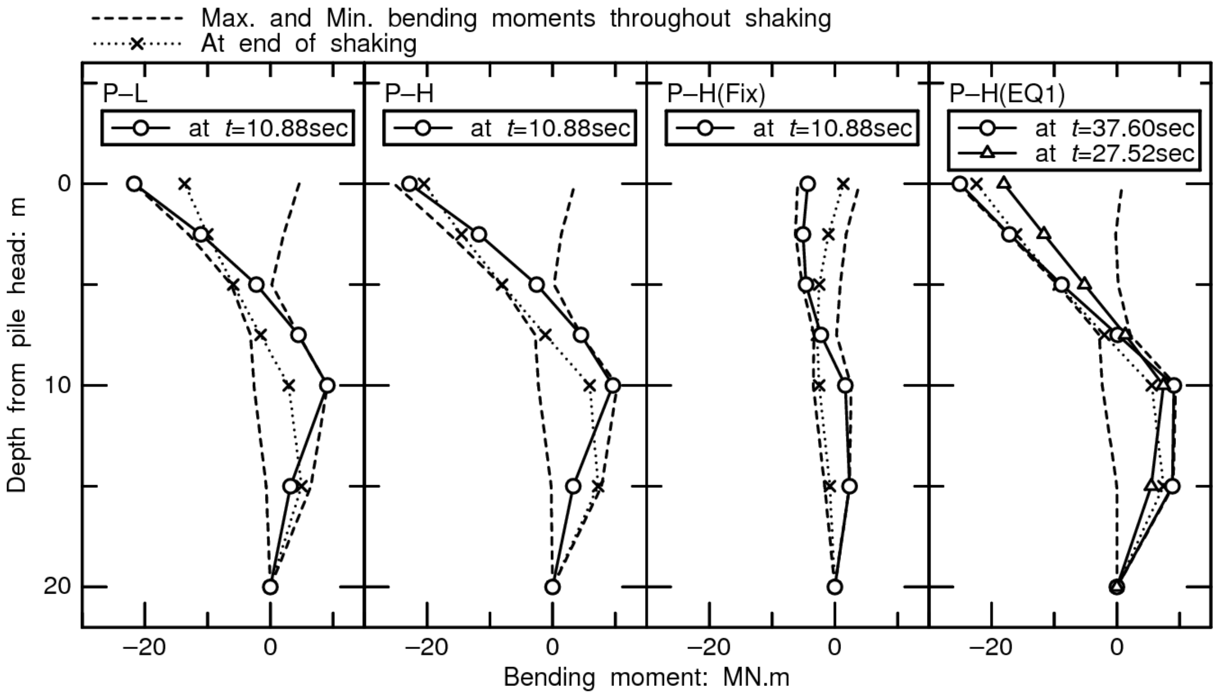

Fig. 10: Distributions of pile bending moment at time of maximum earth pressure acting on abutment back face

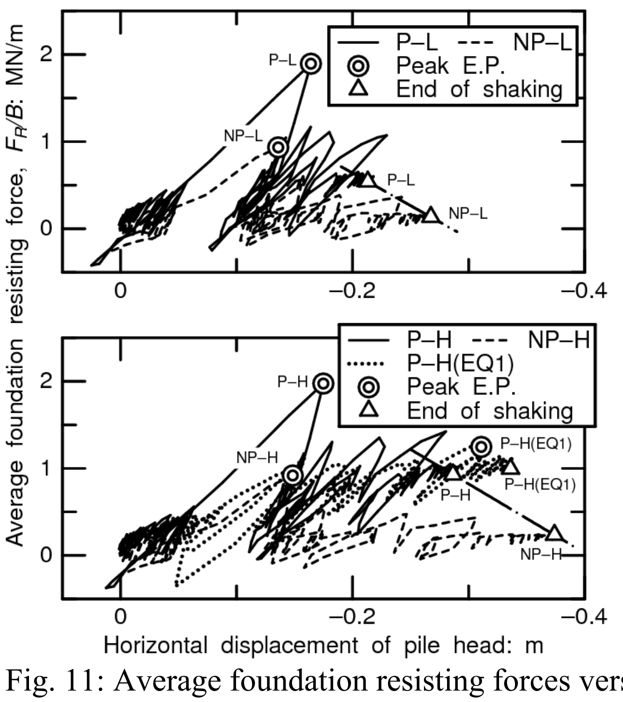

Fig. 11: Average foundation resisting forces versus horizontal displacement of abutment base

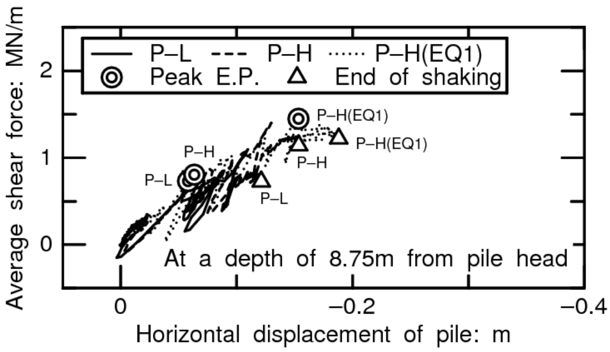

Fig. 12: Average shear forces versus horizontal displacement of piles at a depth of 8.75m

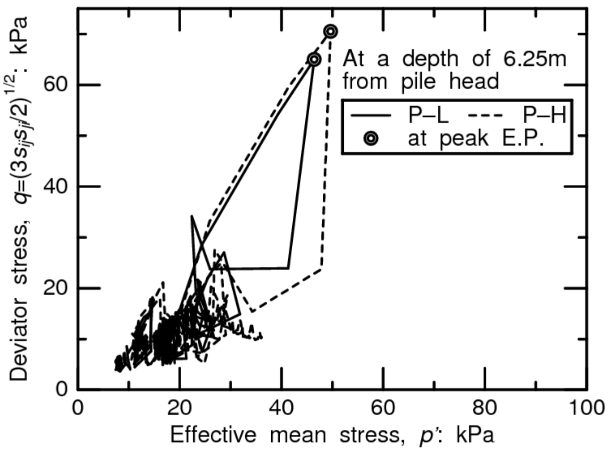

Fig. 13: Stress paths of liquefiable soil element adjacent to pile (x=1.25m, y=3.75m & z=-6.25m) for P-L & P-H

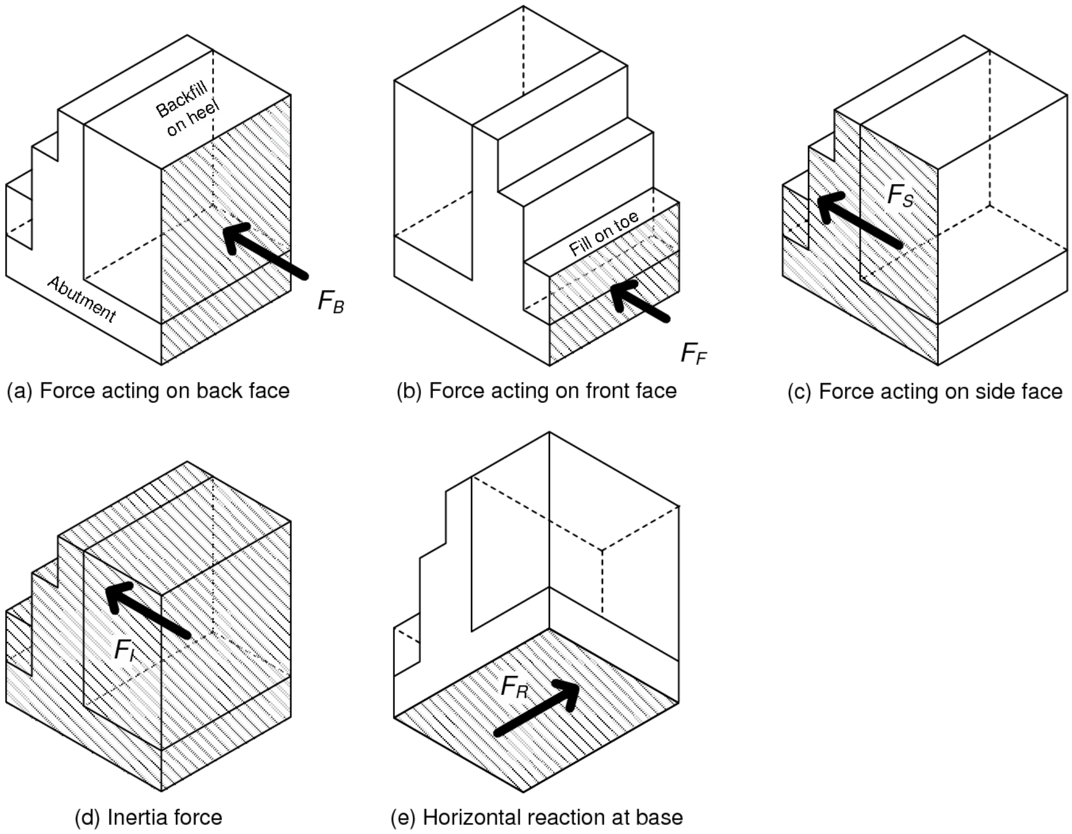

(a) Force acting on back face (b) Force acting on front face (c) Force acting on side face

(d) Inertia force (e) Horizontal reaction at base

Fig. 14: Forces acting on abutment

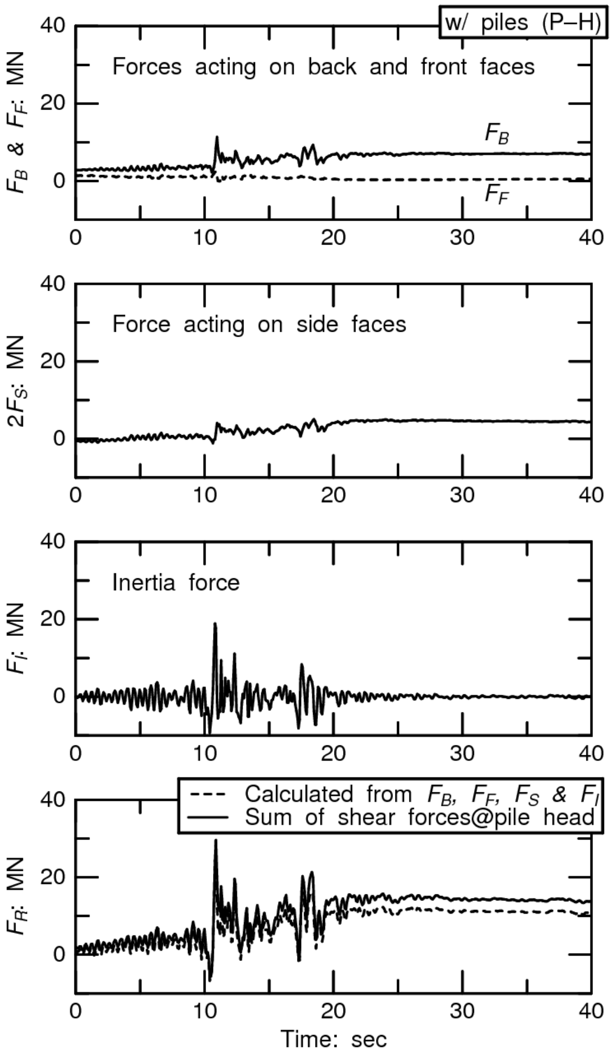

Fig. 15: Changes in forces acting on abutment for P-H

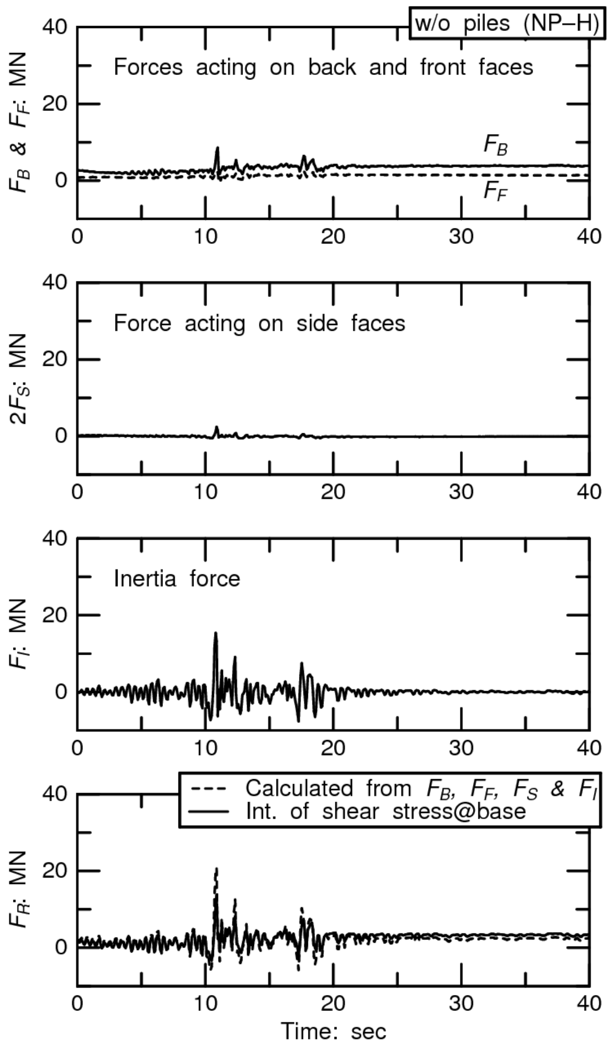

Fig. 16: Changes in forces acting on abutment for NP-H

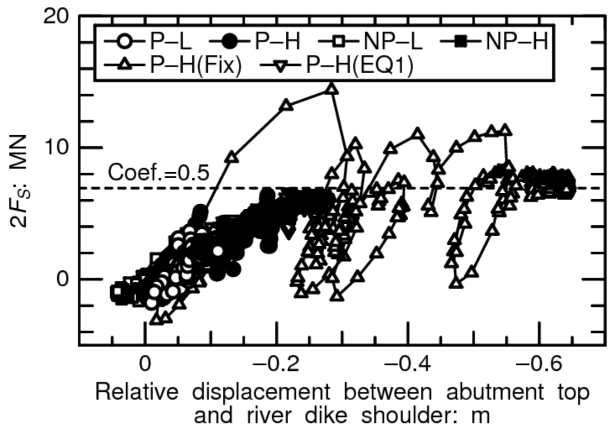

Fig. 17: Forces acting on abutment side faces against relative displacement between abutment and spreading ground